# Measurement of Debye–Waller factors in $Co_3Ti$ by quantitative CBED

M.-Y. Wu,[a,b] S.-Y. Li,[a] Jing Zhu,[a,b]* Z.-H. Du[c] and S.-L. Li[c]

[a]Electron Microscopy Laboratory, School of Materials Science and Engineering, Tsinghua University, Beijing 100084, People's Republic of China, [b]Central Iron and Steel Research Institute, Beijing 100081, People's Republic of China, and [c]Department of Computer Science and Technology, Tsinghua University, Beijing 100084, People's Republic of China. Correspondence e-mail: jzhu@mail.tsinghua.edu.cn

The Debye–Waller factors (DWFs) of Co and Ti atoms in $Co_3Ti$ have been obtained by quantitative convergent-beam electron diffraction (QCBED). They are $B_{Co}$ = 0.20–0.24 and $B_{Ti}$ = 0.41–0.43 Å$^2$ in $Co_3Ti$ at room temperature. A modified simulated-annealing algorithm and its parallel algorithm were employed to obtain reliable results efficiently.

## 1. Introduction

The Debye–Waller factor (DWF) is an important parameter to describe the atomic thermal vibration of materials. Many methods have been proposed in the literature for the calculation or measurement of the DWF.

Theoretically, accurate *ab initio* calculation of the DWFs is difficult, even when the force constants are known, because inharmonic effects must be taken properly into account (Sears & Shelley, 1991). The DWFs can be calculated using the Debye model for an elemental crystal if the Debye temperature is available, but the Debye model does not fit for all temperature ranges (Sears & Shelley, 1991; Peng *et al.*, 1996). More accurate DWFs can be calculated for elemental crystals over a wide temperature range if accurate data on the phonon density of states have been obtained by neutron scattering experiments or the Debye temperature is available (Sears & Shelley, 1991; Peng *et al.*, 1996; Gao & Peng, 1999). For compounds, the DWFs of constituent atoms can be calculated under two conditions. Firstly, the phonon frequencies and displacement eigenvectors for all phonon states can be obtained from a proper model of the lattice dynamics. Secondly, the phonon-dispersion curves of the material must be measured experimentally so that the parameters of the model can be obtained by fitting to the curves. Reid (1983) calculated DWFs for 17 compounds with the zinc-blende structure using several models and Gao & Peng (1999) and Gao *et al.* (1999) have calculated DWFs for 19 compounds with the sodium chloride structure. But for intermetallic materials like $Co_3Ti$, which is of $L1_2$ structure with the lattice parameters $a_0$ = 3.607 Å (Takasugi *et al.*, 1990), it is quite difficult to calculate the DWFs. Up to now, no DWFs of constituent atoms in $Co_3Ti$ are reported.

Experimentally, DWFs can be more accurately measured by X-rays, while methods relating to CBED are more suitable to polycrystals because the electron beam can be converged to as small as 1 nm and it could refine many parameters including DWFs at the same time in the refinement.

Recently, Preston *et al.* (1993) measured DWFs by using a kinematical approximation to study the intensity distribution of high-order Laue-zone (HOLZ) reflections in a CBED pattern. This method worked well for Si but failed for GaAs.

Using zone-axis diffraction, Burgess *et al.* (1994) refined structure factors for Ge with various DWFs and the 'correct' DWF was chosen when the fitted high-order structure factors agreed with the free-atom values.

In view of the important role of DWFs in quantitative CBED pattern matching, Holmestad determined the DWFs of TiAl. They are $B_{Ti}$ = 0.17 and $B_{Al}$ = 0.38 Å$^2$ at 123 K. It has been pointed out that the kinematical approach with the Bethe correction is more accurate than the pure one but can only give an average DWF for different atoms, and the full dynamical calculation is the most accurate (Holmestad, 1994).

More recently, Nüchter *et al.* (1998) have measured temperature factors of NiAl by extracting complete rocking curves of different high-order reflections from one pattern.

## 2. Quantitative CBED method for measuring DWFs

In this paper, the DWFs of Co and Ti atoms in $Co_3Ti$ were measured using two-dimensional quantitative CBED pattern matching. The main procedure for measuring DWFs is similar to the method described by Zhu *et al.* (1997) and Holmestad *et al.* (1993), while three points should be noted. Firstly, the two-dimensional intensity distributions of two high-order reflections have been used as the reference data in the refinement because the high-order reflections are more sensitive to the DWFs. To avoid strong dynamic interactions and bonding effects, high-index zone-axis and off-axis orientations were adopted, where no discs were overlapped (see Fig. 1). Around these orientations, the low-order reflections did not appear or

rarely appeared. Secondly, a modified simulated-annealing optimizing method was employed in the refinement to avoid trapping of the algorithm in local minima. To shorten the computing time, the program was further modified to implement parallel computation on a home-assembled super-computer. Thirdly, individual DWFs were measured for both Co and Ti in $Co_3Ti$.

## 2.1. Experiment

**2.1.1. Preparing the sample for TEM (transmission electron microscope) observation**. Thin foils of $Co_3Ti$ (nominal composition Co–23 at.% Ti) for TEM were prepared by standard twin-jet electron polishing using a 10% $H_2SO_4$–90% $CH_3OH$ electrolyte at 243 K.

**2.1.2. Instrumentation**. A JEOL-2010F transmission electron microscope with a GIF (Gatan image filter) system was used to acquire the two two-dimensional energy-filtered CBED patterns including strong high-order reflections. A $1024 \times 1024$ Gatan model 678 CCD camera with a YAG scintillator was used to record the energy-filtered image. The acceleration voltage was 197.0 kV. An energy window 5 eV around the zero-loss energy was selected. The entrance aperture was about 3 mm in diameter. Convergence angle and probe sizes were carefully chosen for sufficient signal intensity without any disc overlap. A liquid-nitrogen-filled cooling trap was used to minimize thermal diffuse scattering and to reduce contamination.

**2.1.3. Computation environment**. The serial refinement was performed on a SGI O2 workstation while the parallel one was carried on a home-assembled network-based system. In total, eight computers were combined together to form a 'cluster'. Each of the computers is a Dual Pentium III 500 MHz SMP system. The software used was Linux Red Hat 5.1 and MPI CH 1.1.1 Fortran compiler.

## 2.2. Fundamentals

The theoretical intensity distribution in a diffracted disc was calculated based on the Bloch-wave method (Hirsch *et al.*, 1977; Miao *et al.*, 1995; Zhu *et al.*, 1997).

In regard to calculation of the DWFs for a pure $Co_3Ti$ crystal, some of the parameters such as the sample thickness, the incident-beam direction and the DWFs were optimized in the refinement. All these variables were optimized simultaneously because the parameters may interact between each other. In total, nine optimized parameters were included in the refinement: the thickness of the sample, six parameters for incident-beam direction and two parameters for DWFs. The starting values of sample thickness and incident-beam direction were obtained from the same pattern used for DWF determination. The sample thickness was determined by using the fringe profile of the CBED disc (Kelly *et al.*, 1975). As claimed by Holmestad (1994), there are significant systematic errors in this case since the index of the disc used is rather high and the orientation is not strictly two beam. But the errors are reduced by further refinement and then an accurate final value for thickness is obtained. In our experience, accurate deter-

mination of the incident-beam direction is very important. In this paper, the initial incident-beam direction was obtained by the conventional method using three pairs of Kikuchi lines. For optimization of the incident-beam direction, six coordinate parameters were used. The meaning of the parameters ($R1$, $R2$, $g$, phi1, phi2) are shown in Fig. 2. The sixth parameter, which is perpendicular to the paper and not drawn in the figure, describes the deviation angle from the starting zone axis. The ranges of these six parameters were restricted to lie within experimental errors in the refinement processing. The DWFs of the pure elements Co, $B_{Co} = 0.39$ Å$^2$, and Ti, $B_{Ti} = 0.62$ Å, were used as initial DWF values of the Co and Ti atoms in $Co_3Ti$, respectively. The limits on the range of the DWFs were set by the subroutine *ATOM* (Bird & King, 1990) (*i.e.* 0–2.0 Å$^2$) in the refinement processing. This subroutine was also used to calculate the absorption that reflects the diffuse background coming from the phonon scattering.

Because only a finite set of beams can be included in the calculation, the beam-selection method proposed by Zuo & Weickenmeier (1995) was used to automatically select significant reflections during the refinement processing. The number of reflections selected was up to 500 in this work.

## 2.3. Refinement

**2.3.1. Objective function**. The objective function used in the refinement is the NED (normalized Euclidean distance) suggested by Hoffmann *et al.* (1994), *i.e.*

$$\text{NED}(I_1, I_2)$$
$$= \left\{ \sum_{kl} [I_1(r_{kl}) - I_2(r_{kl})]^2 \middle/ \left[ \sum_{kl} I_1^2(r_{kl}) \sum_{kl} I_2^2(r_{kl}) \right]^{1/2} \right\}^{1/2},$$
$$(1)$$

where $I_1$ and $I_2$ denote the normalized experimental and theoretical intensity on the point of $r_{kl}$, respectively. We believe that equation (1) is more objective for the evaluation of the difference of two images than the formalisms used by other authors because it includes no weight coefficient
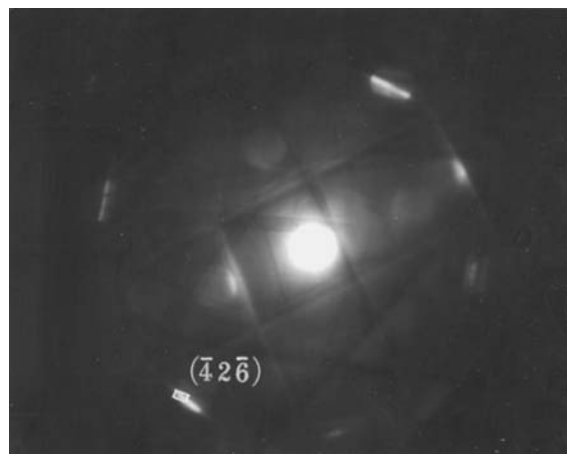


**Figure 1**
An off-axis CBED pattern including strong high-order reflections. (Sample thickness = 130 nm.)

(Nüchter *et al.*, 1998; Holmestad, 1994; Miao *et al.*, 1995; Zuo & Spence, 1991; Deininger *et al.*, 1994).

**2.3.2. Optimization algorithm**. The optimization procedure is a relatively independent part of the procedure. Up to now, several optimization methods have been suggested, such as the simplex method (Zuo & Spence, 1991), conjugate gradients (Marthinsen *et al.*, 1991), quasi-Newton (Bird & Saunders, 1991), non-gradient-based-one-dimensional minimizer (Nüchter *et al.*, 1998), speeded decent + Newton–Raphson (Zhu *et al.*, 1997) and variants of the simulated-annealing algorithm (Deininger *et al.*, 1994). Among these algorithms, only the simulated-annealing method is free from the large number of local minima that appear during refinement. It has been demonstrated that the number of local minima is exceedingly large and increases with increasing number of parameters (Deininger *et al.*, 1994; Li *et al.*, 1999, 2000). In the current work, the simulated-annealing algorithm was used. Furthermore, the algorithm was modified to achieve higher performance according to the special requirements of QCBED (Li *et al.*, 2000). To improve further the efficiency of multidimensional searching, a downhill (Hooke & Jeeves, 1961) calculation was added at each local minimum.

The simulated-annealing algorithm does avoid the local minima, but it requires longer computing time as the number of parameters increases. The parallel algorithm, which performs many more search steps than the serial algorithm in the same computing time was used in this work. The computing time was reduced from about 200 h for the serial algorithm to about 20 h for the parallel algorithm with eight computers.

## 3. Results and discussion

To obtain more convincing results, we processed two reflections: $5\bar{7}\bar{3}$ and $\bar{4}2\bar{6}$. The DWFs were obtained when the objective function NED became very low and would not go

**Table 1**
DWFs ($\mathring{A}^2$) of $Co_3Ti$ at room temperature obtained in the present work.

| Type of atom | From $\bar{4}2\bar{6}$ | From $5\bar{7}\bar{3}$ |
|---|---|---|
| Co | 0.20 | 0.24 |
| Ti | 0.41 | 0.43 |

lower during a certain period of time. Each process cost about 60 000 iterations in total for each computer. Fig. 3 shows the experimental and calculated images of the reflection discs $\bar{4}2\bar{6}$ near the [$76\bar{3}$] zone axis, which gives $B_{Co} = 0.20$ and $B_{Ti} = 0.41 \mathring{A}^2$. Fitting to the $5\bar{7}\bar{3}$ reflection disc gives $B_{Co} = 0.24$ and $B_{Ti} = 0.43 \mathring{A}^2$, but this fitting is not as good as that to $\bar{4}2\bar{6}$ because the experimental pattern has high noises owing to the low counts.

Table 1 shows the experimental DWFs obtained in this work. For the errors produced in the refinement, we speculated that the main error originates from the background of the experimental image. In the current work, only a simple point-spread function was superimposed and the random noise was not considered. Another source of the error of DWF measurement is from the effect of the low-order structure factors. These are not as sensitive to the DWFs and were not optimized in the refinement.

## 4. Conclusions

DWFs of Co and Ti in $Co_3Ti$ have been determined by the quantitative CBED pattern-matching method, $B_{Co} = 0.20–0.24$ and $B_{Ti} = 0.41–0.43 \mathring{A}^2$. The error of measurement is less than 20%. The elastic scattering intensity distribution has been measured using the JEM-2010F with the GIF system attached, the theoretical intensity was calculated based on the many-beam dynamical electron diffraction theory. A modified simulated-annealing algorithm and its parallel algorithm were used during the refinement processing.
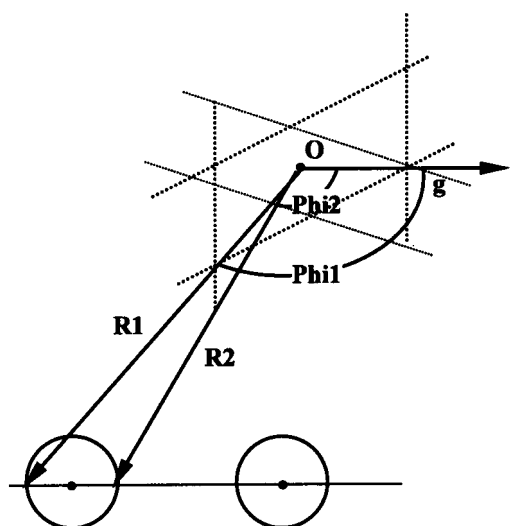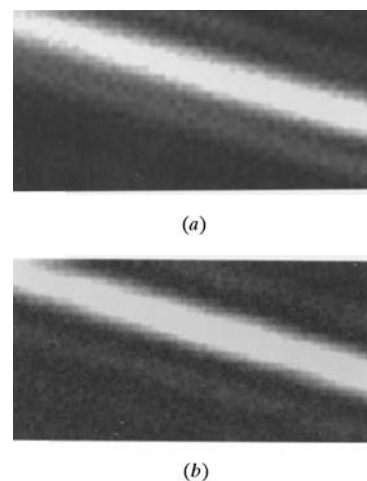


**Figure 2**
The coordinate diagram for the optimization of the incident-beam direction. The letter $O$ marks the center of three Kikuchi pairs.



**Figure 3**
(*a*) The experimental image enlarged from the white block area in Fig. 1. (*b*) The calculated image after refinement.

Wu, Li, Zhu, Du and Li · Debye–Waller factors　**191**

## References

Bird, D. M. & King, Q. Q. (1990). *Acta Cryst.* A**46**, 202–208.

Bird, D. M. & Saunders, M. (1991). *Microbeam Analysis 1991*, edited by D. G. Howitt, pp. 153–156. San Francisco Press.

Burgess, W., Saunders, M., Bird, D. M., Preston, A. R., Zaluzec, N. J. & Humphreys, C. J. (1994). Proc. 13th International Congress on Electron Microscopy, Vol. I, pp. 847–848.

Deininger, C., Necker, G. & Mayer, J. (1994). *Ultramicroscopy*, **54**, 15–30.

Gao, H. X. & Peng, L.-M. (1999). *Acta Cryst.* A**55**, 926–932.

Gao, H. X., Peng, L.-M. & Zuo, J. M. (1999). *Acta Cryst.* A**55**, 1014–1025.

Hirsch, P. S., Howie, A., Nicholson, R. B., Pashley, D. W. & Whelan, M. J. (1977). *Electron Microscopy of Thin Crystals*, pp. 208–219, 276–294. New York: Robert E. Krieger Publishing Co.

Hoffmann, D., Mobus, G. & Ernst, F. (1994). *Ultramicroscopy*, **53**, 205–221.

Holmestad, R. (1994). PhD Dissertation, University of Trondheim-NTH, Norway.

Holmestad, R., Weickenmeier, A. L., Zuo, J. M., Spence, J. C. H. & Horita, Z. (1993). *Inst. Phys. Conf. Ser.* No. 138, pp. 141–144.

Hooke, R. & Jeeves, T. A. (1961). *J. Assoc. Comput. Mach.* **8**, 212–222.

Kelly, P. M., Jostons, A., Blake, R. G. & Napier, J. G. (1975). *Phys. Status Solidi A*, **31**, 771–779.

Li, S. Y., Du, Z. H., Wu, M. Y., Zhu, J. & Li, S. L. (1999). *Int. J. Mod. Phys.* In the press.

Li, S. Y., Wu, M. Y. & Zhu, J. (2000). *Ultramicroscopy*. In the press.

Marthinsen, K., Runde, P., Bakken, L. N. & Høier, R. (1991). *Micr. Microsc. Acta*, **22**, 165–166.

Miao, Y., Zhu, J., Lin, X. W. & Jiang, W. J. (1995). *J. Mater. Res.* **10**, 1913–1916.

Nüchter, W., Weickenmeier, A. L. & Mayer, J. (1998). *Acta Cryst.* A**54**, 147–157.

Peng, L. M., Ren, G., Dudarev, S. L. & Whelan, M. J. (1996). *Acta Cryst.* A**52**, 456–470.

Preston, A. R., Burgess, W. G., Pickup, C. J. & Humphreys, C. J. (1993). *Inst. Phys. Ser.* No. 138, Section 3, pp. 145–148.

Reid, J. S. (1983). *Acta Cryst.* A**39**, 1–13.

Sears, V. F. & Shelley, S. A. (1991). *Acta Cryst.* A**47**, 441–446.

Takasugi, T., Takazawa, M. & Izumi, O. (1990). *J. Mater. Sci.* **25**, 4226–4230.

Zhu, J., Miao, Y. & Guo, J. T. (1997). *Acta Mater.* **45**, 1989–1994.

Zuo, J. M. & Spence, J. C. H. (1991). *Ultramicroscopy*, **35**, 185–196.

Zuo, J. M. & Weickenmeier, A. L. (1995). *Ultramicroscopy*, **57** 375–383.